The Astrophysical Journal, 940:80 (6pp), 2022 November 20 https://doi.org/10.3847/1538-4357/ac9c65

Polarization Observations of a Split-band Type II Radio Burst from the Solar Corona

R. Ramesh and C. Kathiravan
Indian Institute of Astrophysics, Koramangala 2nd Block, Bangalore 560034, Karnataka, India
Received 2022 August 11; revised 2022 October 7; accepted 2022 October 16; published 2022 November 23

Abstract

Using temporal observations of circular polarized harmonic plasma emission from a split-band type II solar radio burst at 80 MHz, we separately estimated the coronal magnetic field strengths (B) associated with the lower (L) and upper (U) frequency bands of the burst. The corresponding Stokes I and V data were obtained with the polarimeter operating at the above frequency in the Gauribidanur observatory. The burst was associated with a flare/coronal mass ejection on the solar disk. Simultaneous spectral observations with the spectrograph there in the frequency range 80–35 MHz helped to establish that the observed polarized emission was from the harmonic component of the burst. The B values corresponding to the polarized emission from the L and U bands at 80 MHz are $B_L \approx 1.2$ G and $B_U \approx 2.4$ G, respectively. The different values of B for the observed harmonic emission at the same frequency (80 MHz) from the two bands imply unambiguously that the corresponding fundamental emission at 40 MHz must have originated at different spatial locations. Two-dimensional radio imaging observations of the burst with the radioheliograph in the same observatory at 80 MHz indicate the same. As comparatively higher B is expected behind a propagating shock due to compression as well as the corresponding coronal regions being closer to the Sun, our results indicate that the sources of L- and U-band emission should be located ahead of and behind the associated coronal shock, respectively. These are useful to understand the pre- and postshock corona as well as locations of electron acceleration in a propagating shock.

Unified Astronomy Thesaurus concepts: Solar corona (1483); The Sun (1693); Radio bursts (1339); Polarimetry (1278); Solar coronal mass ejections (310); Solar flares (1496); Solar magnetic fields (1503)

1. Introduction

Solar type II radio bursts are signatures of magnetohydrodynamic (MHD) shocks propagating outwards through the solar atmosphere. The electrons accelerated at the MHD shocks give rise to plasma oscillations that are converted into escaping radio emission. Coronal mass ejections (CMEs), flares, and various types of ejecta are considered to be responsible for the aforementioned shocks. The electron density (N_e) and hence the plasma frequency (f_p) decreases with increasing heliocentric distance (r). Due to this the type II bursts show frequency drift as a function of time. The drift rate is $\lesssim$1 MHz s^{-1}. The detailed characteristics of type II bursts could be found in Nelson & Melrose (1985), Mann et al. (1995), Aurass (1997), Gopalswamy (2006), and Nindos et al. (2011). Spectral observations show that type II bursts usually occur as fundamental (F) and harmonic (H) bands. The frequency ratio is ≈1:2 for the two bands. In some situations, either or both the bands are split into two subbands: lower (L) and upper (U). Their frequency separation is smaller than that between the F and H bands. Smerd & Stewart (1974), Smerd et al. (1975), and Vrsnak et al. (2001) attributed the L and U bands to emission originating simultaneously from the coronal regions ahead of and behind the propagating MHD shock, respectively. These are also called the upstream (L) and downstream (U) regions of the shock. At any given time, radio emission from the shock upstream and downstream would be at lower and higher frequencies. Hence the labels L and U, respectively. According to another interpretation, the band split could be explained by similar simultaneous emission from coronal regions ahead of two different parts of the shock (McLean 1967; Holman & Pesses 1983; Knock et al. 2003; Knock & Cairns 2005). Two-dimensional images of split-band type II radio bursts reported (Nelson & Sheridan 1974; Nelson & Robinson 1975) revealed that the L- and U-band sources are spatially separated even at the same frequency, be it the F or H component. The observations were primarily at 43 and 80 MHz. Zimovets et al. (2012), Zimovets & Sadykov (2015), and Zucca et al. (2014) showed that the L-band source was located above the U-band source at any given moment in the frequency range ≈150–450 MHz. Even at the same frequency, the centroids of the L- and U-band sources were distinctly separate. Chrysaphi et al. (2018) pointed out that the spatial separation between the L- and U-band sources observed by them in the frequency range ≈30–42 MHz could be explained as due to scattering of radio waves by the coronal density inhomogeneities (Aubier et al. 1971; Thejappa & Kundu 1991; Sastry 1994; Ramesh et al. 2006a; Mugundhan et al. 2017; Ramesh et al. 2020b; Zhang et al. 2022). But, observations at frequencies like 150–450 MHz mentioned above should be less affected by scattering and other propagation effects as compared to lower frequencies (Aubier et al. 1971; Bastian 2004; Thejappa & MacDowall 2008). Even at low frequencies, sources of angular sizes lesser than that predicted by scattering calculations have been observed (Ramesh et al. 1999b; Ramesh & Sastry 2000; Ramesh & Ebenezer 2001; Kathiravan et al. 2011; Ramesh et al. 2012b; Mugundhan et al. 2016; Mugundhan et al. 2018a). These indicate that the issue related to the source locations of either bands in a split-band type II solar radio burst is still open. So, we were interested to investigate the problem using polarization observations since the strength of the magnetic field associated with the L- and U-band sources could be inferred independently, which in turn might help to understand whether

the sources are cospatial or not. There are several estimates of B using the density jump across the shock derived using total intensity observations of split-band type II bursts (see, e.g., Vrsnak et al. 2002; Gopalswamy et al. 2012; Kishore et al. 2016 and the references therein). But, they correspond to the upstream corona in general. Note that plasma emission in a magnetic field gets split as ordinary (O) and extraordinary (X) modes. Since the propagation characteristics of these two modes are different, there will be a resultant circular polarization (Melrose & Sy 1972). In the case of harmonic plasma emission, the associated B can be estimated in a relatively simple manner (see, e.g., Melrose et al. 1980; Zlotnik 1981). Polarization of the harmonic plasma emission is also minimally affected by propagation effects (Dulk & McLean 1978). Observations of circular polarization of type II radio bursts are known since the time the bursts were discovered (Komesaroff 1958; Roberts 1959; Stewart 1966; Suzuki et al. 1980; Cairns & Robinson 1987; Thejappa et al. 2003; Du et al. 2014; Alissandrakis et al. 2021). There are also estimates of B using observations of weak circular polarized emission from harmonic type II bursts (Hariharan et al. 2014; Kumari et al. 2017a, 2019; Ramesh & Kathiravan 2022b). But, information on the B values corresponding to the individual bands in a split-band type II burst are rare. Such results are useful to understand the source regions of the two bands with respect to the associated shock. Hence the present work.

2. Observations

The polarization data were obtained with the Gauribidanur Radio Interferometer Polarimeter (GRIP; Ramesh & Sastry 2005; Ramesh et al. 2008) at 80 MHz. The GRIP is operated by the Indian Institute of Astrophysics in the Gauribidanur Observatory located about 100 km north of Bangalore (Ramesh 2011; Ramesh et al. 2014). It is an east–west one-dimensional interferometer array of 40 log-periodic dipole antennas (LPDA; Ramesh et al. 1998), and simultaneously observes the circularly polarized and total flux densities from the "whole" Sun. Linear polarization, if generated at the corresponding radio source region in the solar atmosphere, gets canceled out in the corona itself due to the physical properties of the medium (Grognard & McLean 1973; Morosan et al. 2022). The half-power width of the GRIP response pattern near the zenith is $\approx 1.^{\circ}5 \times 90^{\circ}$ (R.A., R.A.$\times$ decl., decl.) at the above frequency. This implies that Sun is a "point" source for observations with the GRIP. For radio spectral data, we used observations with the Gauribidanur Low-frequency Solar Spectrograph (GLOSS) in the frequency range 85–35 MHz (Ebenezer et al. 2001, 2007; Kishore et al. 2014; Hariharan et al. 2016b). It is a one-dimensional array of eight LPDAs set up along a north–south baseline in the total power mode. The half-power width of the response pattern of GLOSS for observations near the zenith is $\approx 90^{\circ} \times 6^{\circ}$ (R.A.$\times$ decl.) at the highest frequency of operation, i.e., 85 MHz. While the width of the response pattern along R.A. is nearly independent of frequency, its width along the decl. varies inversely with the frequency. A field programmable gate array based digital backend receiver system was used for simultaneous data acquisition at all the frequencies in the aforementioned frequency range. The sampling rate was $\approx$1 GHz. The spectral bandwidth and integration time are $\approx$1 kHz and $\approx$256 ms, respectively (Mugundhan et al. 2018b; Bane et al. 2022). The two-dimensional radio images were obtained with the Gauribidanur Radioheliograph (GRAPH) at 80 MHz (Ramesh et al. 1998, 1999a, 2006b). The GRAPH is a t-shaped radio interferometer array of 384 LPDAs. Its angular resolution for observations close to the zenith is $\approx 4' \times 6'$ (R.A. $\times$ decl.) at the above frequency. The integration time is $\approx$ 250 ms and the observing bandwidth is $\approx$ 2 MHz. We also used data obtained with the Gauribidanur Radio Spectro-Polarimeter (Sasikumar Raja et al. 2013a; Hariharan et al. 2015; Kishore et al. 2015; Mugundhan et al. 2018b), and e-CALLISTO (Monstein et al. 2007; Benz et al. 2009). For information on CMEs, we used the catalog generated from observations in whitelight with the Large Angle and Spectrometric Coronagraph C2 (LASCO-C2; Brueckner et al. 1995) onboard the Solar and Heliospheric Observatory (SOHO).[1]

Figure 1 shows the GLOSS observations of an F–H type II burst from the solar corona on 2021 May 22 in the time interval $\approx$ 02:57–03:09 UT. Both the F and H emission show clear split-band characteristics. $F_L(H_L)$ and $F_U(H_U)$ are the lower and upper bands in the F(H) emission, respectively. The shock speed estimated from the H component of the type II burst using the Vrsnak et al. (2004) model for the N_e distribution in the solar corona is ≈ 692 km s^{-1}. The corresponding value for the F component is ≈ 1115 km s^{-1}. The burst was associated with a 1N class H alpha flare observed during the interval $\approx$ 02:51–03:05 UT, with maximum emission at $\approx$ 02:55 UT. The heliographic coordinates of the flare location were N17E37.[2] There was also a C6.1 class GOES soft X-ray flare in the time range $\approx$ 02:47–03:00 UT with peak emission at $\approx$02:56 UT. An inspection of the SOHO/LASCO catalog indicates that a CME was noticed around $\approx$ 04:00 UT on 2021 May 22 with a leading edge (LE) at $r \approx 2.7\ R_{\odot}$. Its central position angle (measured counterclockwise from the solar north) and angular width were $\approx 81^{\circ}$ and $\approx 79^{\circ}$, respectively. The narrow bandwidth of the type II burst is reasonably consistent with the latter (see, e.g., Ramesh et al. 2022a). The CME had a linear speed of ≈ 366 km s^{-1} and an acceleration of $\approx$84m s^{-2} in the SOHO/LASCO-C2 field of view. Figure 2 shows the GRIP observations of Stokes I and V emission associated with the above type II burst at 80 MHz over the period $\approx$03:00–03:03 UT. There were no GRIP observations prior to $\approx$ 03:00 UT. A comparison of Figures 1 and 2 indicates that the first and second maxima (peaks) in Figure 2 correspond to the L and U bands at 80 MHz in the H component of the split-band burst in Figure 1. Accordingly, we marked the two peaks in Figure 2 as H_L and H_U, respectively. The time interval between them is $\approx$2 minutes. The peak flux densities of their Stokes I emission are $\approx$38,133 Jy (H_L) and 11,000 Jy (H_U), where 1 Jy$=10^{-26}$ Wm^{-2} Hz^{-1}. These are in the range of flux density values reported in the literature for type II burst observations at 80 MHz (Nelson & Melrose 1985). The peak flux densities of the Stokes V emission in Figure 2 are $\approx$1851 Jy (H_L) and 1118 Jy (H_U). Therefore, the peak degrees of circular polarization ($dcp = |V|/I$) are ≈ 0.05 (H_L) and 0.10 (H_U), respectively.

3. Analysis and Results

The observations described in Section 2 clearly indicate that the GRIP observations of the type II bursts in Figure 2 are due to harmonic plasma emission. So, we estimated the B near the

[1] https://cdaw.gsfc.nasa.gov/CME_list
[2] https://ftp.swpc.noaa.gov/pub/warehouse/

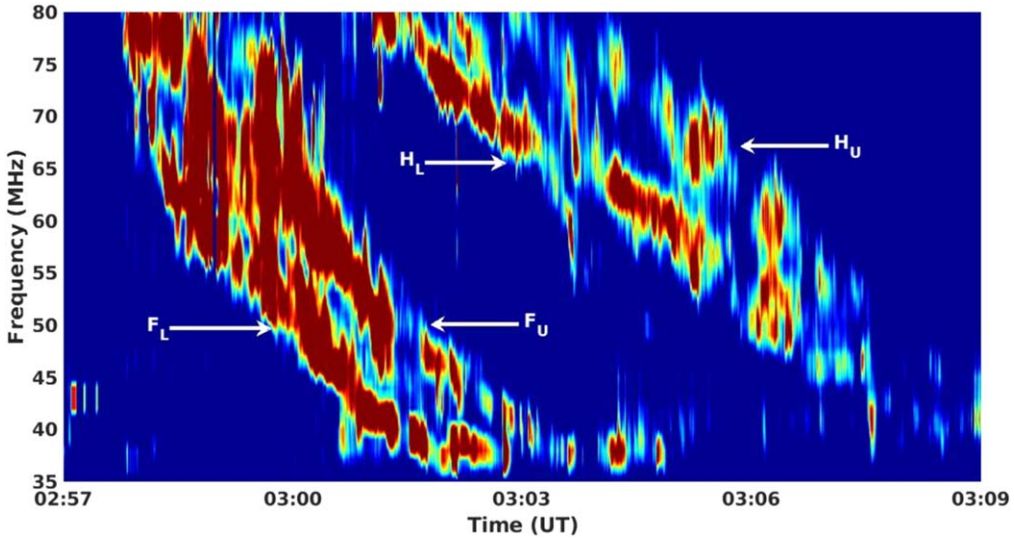

Figure 1. F–H split-band type II burst observed with the GLOSS on 2021 May 22. The high and low frequency cutoff near ≈80 and 35 MHz in the spectrum are due to the use of low and high pass filters to suppress radio frequency interference above and below the respective frequencies.

source region of the bursts using the following relation $B = \frac{f_p \times dcp}{2.8a(\theta)}$ (Melrose et al. 1980). Note that the *dcp* values in the present case are $\lesssim$0.1 (see Section 2). Since the aforementioned formula based on simplifying assumptions like head-on Langmuir wave coalescence is valid for $dcp \lesssim 0.16$ (Willes & Melrose 1997), we are justified in using the same to calculate B; $a(\theta)$ is a slowly varying function of the angle θ between the magnetic field and the viewing direction; f_p is in units of MHz and it corresponds to the fundamental plasma frequency; θ can be approximated to the heliographic longitude of the associated active region (Dulk & Suzuki 1980). Therefore, $\theta \approx 37°$ in the present case (see Section 2). We assumed $a(37°) \approx 0.6$ as mentioned in Dulk & McLean (1978). Substituting this and $f_p = 40$ MHz in the above relation, we find that $B_L \approx 1.2$ G and $B_U \approx 2.4$ G for the *dcp* values of ≈ 0.05 and 0.10 corresponding to the peak H_L and H_U, respectively (see Section 2). The *dcp* and hence B values are different though f_p is the same. This indicates that the *L*- and *U*-band sources related to the observations in Figure 2 must be at different locations. Two-dimensional synthesis imaging observations of the bursts with the GRAPH in the total intensity mode at 80 MHz during the interval ≈ 03:01–03:03 UT is in support of the above argument (Figure 3). An inspection of Figure 2 indicates that there was no other intense emission during the above period. Note that any scattering related changes in the size or position are expected to be similar for both the sources in Figure 3. It is the same for the case with possible projection effects also. We want to add here that even if there is any error in our assumed values for $a(\theta)$, B_U would still be $\approx 2\times$ more compared to B_L. Furthermore, any center-to-limb effects on the B_L and B_U values should be also minimal since their source regions were closer to the disk center.

Bemporad & Mancuso (2010) and Su et al. (2022) showed that B in the downstream region of the coronal shock is $\approx 2\times$ enhanced as compared to its upstream region due to compression of the coronal plasma by the shock. In the present case, $B_U \approx 2B_L$ for observations at the same frequency (80 MHz). This indicates that the respective emission should have been from downstream (*U* band) and upstream (*L* band) of the associated shock. The possibility of both the *L*- and *U*-band emission occurring in the upstream corona itself from two different regions is less likely since the corresponding B values would be nearly equal in such a case (Bemporad et al. 2014). The shock will have a certain width. This implies that during propagation its upper and lower boundaries (in the direction of the observer) will be at the plasma layer (corresponding to the observing frequency) at different epochs. So, even if the electron acceleration responsible for the observed emission were to occur at the respective surfaces (boundaries) of the shock, there should be a finite time interval between the observations of the *L*- and *U*-band emission at the same frequency. The GRIP observations in Figure 2 are consistent with this scenario. Multiplying the time interval (≈2 minutes) between the H_L and H_U bands in the GRIP observations with the estimated shock speed of the F component of the burst in Figure 1, i.e., $\approx 1115\ \mathrm{km\ s^{-1}}$ (since the corresponding plasma layers are where the Langmuir oscillations would be excited as the shock propagates outward), we get the distance (d) traveled by the shock as $\approx 0.2\ R_\odot$ in the above time interval. We carried out similar calculations with the shock speed derived using other N_e models for the solar corona also. The minimum values for the aforementioned speed and distance were in the case of the Newkirk (1961) model. The corresponding values are $\approx 814\ \mathrm{km\ s^{-1}}$ and $\approx 0.14\ R_\odot$, respectively. Even this minimum d is larger than the typical thickness (≈ 0.02–$0.04\ R_\odot$) of the whitelight shock (Bemporad & Mancuso 2010; Eselevich & Eselevich 2012; Gopalswamy et al. 2012). Therefore, the *L*- and *U*-band emission need not be strictly due to electron acceleration at the upper and lower boundaries of the propagating shock as mentioned above. In the case of the *U*-band emission, it could be from anywhere in the downstream corona (in the standoff distance between the shock and the LE of the eruption/flux rope/CME) from where the emission generated at the observing frequency is able to propagate outside (see, e.g., Zimovets et al. 2012). The aforesaid standoff distance is expected to increase as a function of r (Gopalswamy et al. 2012). In summary, the sources of *L*- and *U*-band emission could be either above and below the nose or flank or nose and flank of the shock, irrespective of whether their frequencies are the same or different. In all of the above cases, the *L*- and *U*-band sources would be at different spatial

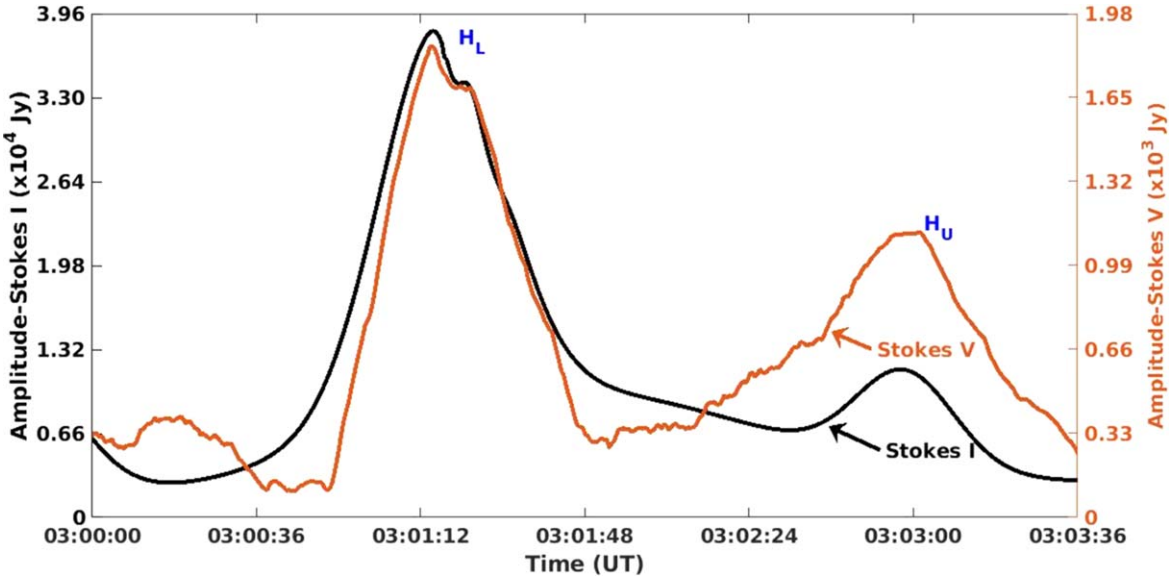

Figure 2. GRIP observations of Stokes *I* and *V* emission at 80 MHz corresponding to the H_L and H_U bands in Figure 1. Note that the Stokes *I* and *V* amplitude values are marked on the left and right-hand side ordinate axes, respectively.

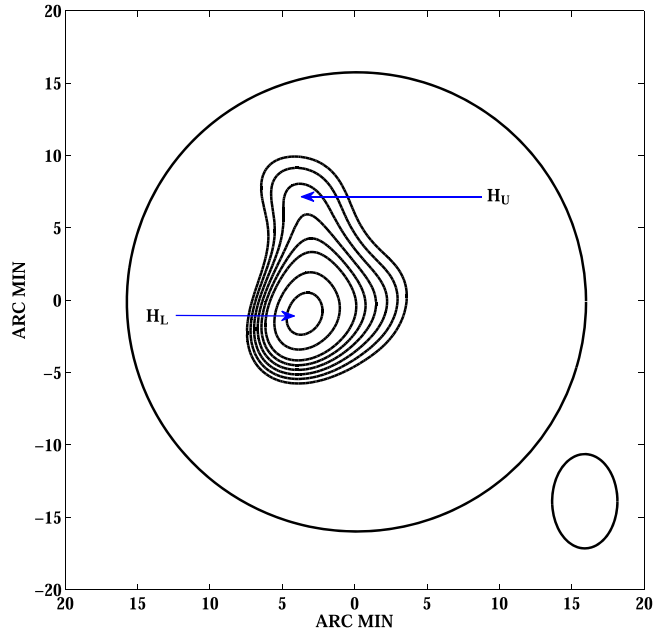

Figure 3. GRAPH observations of the total intensity emission at 80 MHz during the interval ≈ 03:01–03:03 UT, the same period as the H_L and H_U band observations in Figure 2. The circle represents the limb of the Sun's photosphere. Solar north is straight up and east is to the left in the image. The GRAPH "beam" at 80 MHz is shown near the lower right corner. The peak brightness temperature (T_b) is $\approx 8.2 \times 10^7$ K, and it corresponds to the southern source. A comparison with the Stokes *I* observations in Figure 2 indicates that the intense (faint) source to the south (north) corresponds to the H_L (H_U) emission shown there.

locations and heliocentric distances. Differences in the refraction (due to density gradient) suffered by the two sources could also add to the observed spatial separation since propagation of radio emission from the *U*-band source will experience a sudden decrease in density at the corresponding plasma layer due to compression behind the shock. Note that in the above arguments we have assumed that the other coronal conditions for the generation of the type II bursts in the downstream and upstream corona are satisfied (Mann et al. 1995; Vrsnak et al. 2001; Jebaraj et al. 2021; Kouloumvakos et al. 2021).

The mean location of the 40 MHz plasma layer as per the commonly used N_e models for the solar corona is $r \approx 1.60 \pm 0.18$ $R_\odot$ (Baumbach 1937; Allen 1947; Newkirk 1961; Saito et al. 1977; Vrsnak et al. 2004). Combining the above with the distance of ≈ 0.2 $R_\odot$ traveled by the shock in the ≈2 minutes time interval between the peak H_L and H_U emission at 80 MHz in Figure 2, we find that the source regions of their corresponding fundamental emission at 40 MHz should be at ≈1.6 $R_\odot$ (F_L) and 1.4 $R_\odot$ (F_U), respectively. The estimated *B* values at the above locations are $B_L \approx 1.2$ G (1.6 $R_\odot$) and $B_U \approx 2.4$ G (1.4 $R_\odot$). For comparison, the *B* values at the above two locations according to the widely referred Dulk & McLean (1978) model are ≈1.1 G (1.6 $R_\odot$) and 2.0 G (1.4 $R_\odot$). Corresponding values obtained from the independent statistical work of Mancuso et al. (2003) are ≈1.1 G and 1.8 G, respectively. The above predicted values for $r \approx 1.6$ $R_\odot$ agree closely with our estimate of B_L at the same *r*. But the predictions for $r \approx 1.4$ $R_\odot$ are lesser than B_U at the same *r*. This difference is presumably because B_U corresponds specifically to the downstream corona behind the shock where there could be enhancement in the magnetic field due to compression (Bemporad & Mancuso 2010). We would like to add here that there are several estimates of *B* from observations of similar split-band type II bursts. But, they are based on a density jump across the shock, and limited to the upstream corona as mentioned earlier. Figure 4 shows some of the values at particularly $r \approx 1.6$ $R_\odot$, i.e., ≈ 2.8–3.2 G (Smerd et al. 1975), ≈ 1–7 G (Vrsnak et al. 2002), ≈1.2 G (Cho et al. 2007), ≈ 0.7–0.9 G (Gopalswamy et al. 2012), ≈1.3–1.7 G (Kishore et al. 2016), and ≈ 1.9 G (Mancuso et al. 2019). Similar density jump calculations with type I burst chain data indicates ≈ 0.6 G (Gopalswamy et al. 1986). We used the above method for the present event also to verify our estimate of B_L from the polarization data. An inspection of Figure 2 indicates that at ≈ 03:01 UT, the lower and upper frequencies in the F component of the type II burst are at ≈ 40 and 55 MHz, respectively. Note that we chose the above epoch since

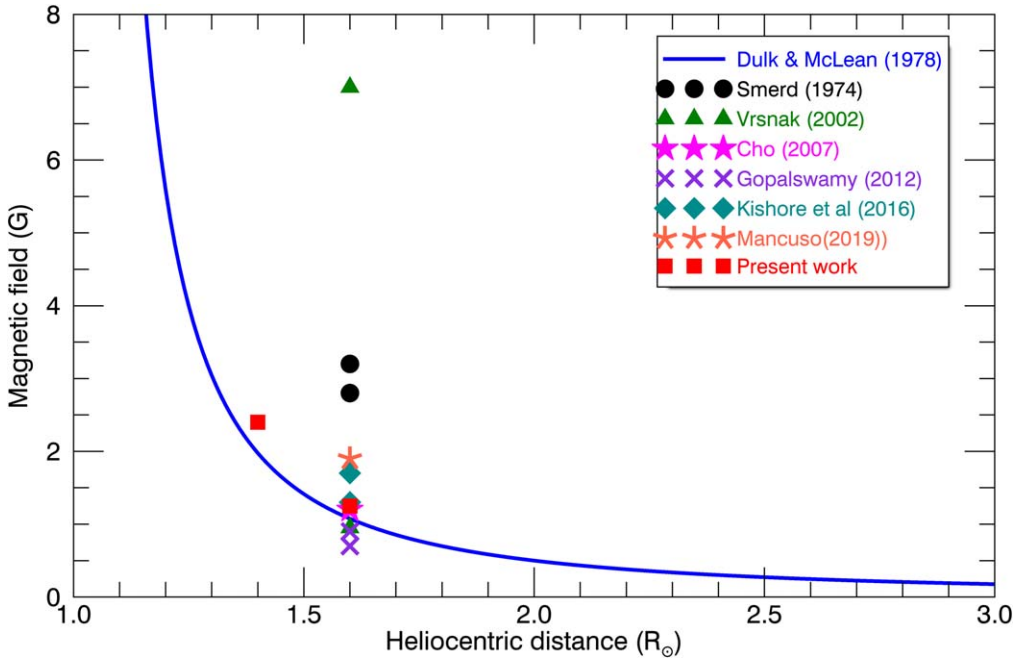

Figure 4. Estimates of B at $r \approx 1.6\ R_\odot$ in the upstream corona ahead of a propagating MHD shock in the solar corona using observations of split-band type II bursts and the density jump across the shock. Red color square symbols represent the B values in both the upstream ($r \approx 1.6\ R_\odot$) and downstream ($r \approx 1.4\ R_\odot$) corona (with respect to the associated shock) from the circular polarization measurements in the present work. The blue color line like shows the Dulk & McLean (1978) model for the variation of B with r obtained from observations of different types of solar radio bursts.

$F_L \approx 40$ MHz and hence the calculations of B will correspond to $r \approx 1.6\ R_\odot$ in the upstream corona similar to the polarization measurements mentioned above. The shock parameters calculated from the spectral observations following the steps described in Kishore et al. (2016) are instantaneous bandwidth ≈ 0.38, density jump (X) ≈ 1.9, Alfvén-Mach number (M_A) ≈ 1.8, and Alfvén speed (v_A) $\approx 619\ \mathrm{km\ s^{-1}}$. These are consistent with the similar values reported in the literature (see, e.g., Vrsnak et al. 2002). From the above numbers, we obtained $B_L \approx 1.3$ G at $r \approx 1.6\ R_\odot$. This is almost equal to the corresponding estimate using the observed circular polarization of the type II burst (i.e., $B_L \approx 1.2$ G at the same r). This consistency in the estimates of B_L using two different radio techniques is encouraging. Furthermore, it reinforces our result for B_U from polarization observations in the present case.

4. Conclusions

We observed a F–H split-band type II burst from the solar corona on 2021 May 22 with heliograph (80 MHz), spectrograph (35–80 MHz), and polarimeter (80 MHz) in the Gauribidanur observatory. Our results indicate that the emission from the L and U bands belonging to the H component of the burst at 80 MHz originated from different locations with different B. The sources with lower and higher B are from the upstream and downstream corona of the associated MHD shock, respectively. More observations of similar events in the future, particularly in the two-dimensional spectro-polarimetric imaging mode, are needed to understand the source regions of the split-band type II bursts associated with the coronal MHD shocks and their plasma characteristics (see, e.g., Bemporad et al. 2014). This is important since: (i) circular polarization observations of harmonic plasma emission helps to derive B independent of any assumption for $N_e(r)$ and hence the speed of the propagating disturbance, which have been mentioned as some of the shortcomings in the upstream/downstream scenario explanation for split-band type II bursts (Du et al. 2015). Information about $N_e(r)$ is required only to establish the r of the observed radio emission; (ii) there are differing views on the radio emission downstream of a shock wave in the case of in situ observations near 1 au (see Vrsnak et al. 2001; Zimovets et al. 2012 and the references therein). Coordinated Stokes I and V observations with the Parker Solar Probe (see, e.g., Pulupa et al. 2020) should help to resolve this. High cadence complementary whitelight observations in the range $r \lesssim 3\ R_\odot$ (where the low frequency coronal type II radio bursts as reported in the current work generally occur) with the Visible Emission Line Coronagraph (Singh et al. 2011) on board ADITYA-L1, the soon to be launched first Indian space solar mission, are also expected to be helpful in this connection.

We are grateful to Gauribidanur Observatory team for their help in the observations and upkeep of the facilities. Indrajit V. Barve, K. P. Santosh, and M. Rajesh are acknowledged for their assistance to the present work. We thank the referee for their comments that helped to us to describe the results more clearly.

ORCID iDs

R. Ramesh https://orcid.org/0000-0003-2651-0204
C. Kathiravan https://orcid.org/0000-0002-6126-8962

References

Allen, C. W. 1947, MNRAS, 107, 426
Alissandrakis, C. E., Nindos, A., Patsourakos, S., & Hillaris, A. 2021, A&A, 654, A112
Aubier, M., Leblanc, Y., & Boischot, A. 1971, A&A, 12, 435
Aurass, H. 1997, in Coronal Physics from Radio and Space Observations, ed. G. Trottet, Vol. 483 (Berlin: Springer), 135

Bane, K. S., Barve, I. V., Gireesh, G. V. S., Kathiravan, C., & Ramesh, R. 2022, JATIS, 8, 017001
Bastian, T. S. 2004, P&SS, 52, 1381
Baumbach, S. 1937, AN, 263, 121
Bemporad, A., & Mancuso, S. 2010, ApJ, 720, 130
Bemporad, A., Susino, R., & Lapenta, G. 2014, ApJ, 784, 102
Benz, A. O., Monstein, C., Meyer, H., et al. 2009, EM&P, 104, 277
Brueckner, G. E., Howard, R. A., Koomen, M. J., et al. 1995, SoPh, 162, 357
Cairns, I. H., & Robinson, R. D. 1987, SoPh, 111, 365
Cho, K.-S., Lee, J., Gary, D. E., Moon, Y.-J., & Park, Y. D. 2007, ApJ, 665, 799
Chrysaphi, N., Kontar, E. P., Holman, G. D., & Temmer, M. 2018, ApJ, 868, 79
Du, G., Chen, Y., Lv, M., et al. 2014, ApJL, 793, L39
Du, G., Kong, X., Chen, Y., et al. 2015, ApJ, 812, 52
Dulk, G. A., & McLean, D. J. 1978, SoPh, 57, 279
Dulk, G. A., & Suzuki, S. 1980, A&A, 88, 203
Ebenezer, E., Ramesh, R., Subramanian, K. R., SundaraRajan, M. S., & Sastry, C. 2001, A&A, 367, 1112
Ebenezer, E., Subramanian, K. R., Ramesh, R., Sundara Rajan, M. S., & Kathiravan, C. 2007, BASI, 35, 111
Eselevich, V., & Eselevich, M. 2012, ApJ, 761, 68
Gopalswamy, N. 2006, GMS, 165, 207
Gopalswamy, N., Nitta, N., Akiyama, S., Makela, P., & Yashiro, S. 2012, ApJ, 744, 72
Gopalswamy, N., Thejappa, G., Sastry, C. V., & Tlamicha, A. 1986, BAICz, 37, 115
Grognard, R. J. M., & McLean, D. J. 1973, SoPh, 29, 149
Hariharan, K., Ramesh, R., & Kathiravan, C. 2015, SoPh, 290, 2479
Hariharan, K., Ramesh, R., Kathiravan, C., Abhilash, H. N., & Rajalingam, M. 2016b, ApJS, 222, 21
Hariharan, K., Ramesh, R., Kishore, P., Kathiravan, C., & Gopalswamy, N. 2014, ApJ, 795, 14
Holman, G. D., & Pesses, M. E. 1983, ApJ, 267, 837
Jebaraj, I. C., Kouloumvakos, A., Magdalenić, J., et al. 2021, ApJ, 654, A64
Kathiravan, C., Ramesh, R., Barve, I. V., & Rajalingam, M. 2011, ApJ, 730, 91
Kishore, P., Kathiravan, C., Ramesh, R., Rajalingam, M., & Barve, I. V. 2014, SoPh, 289, 3995
Kishore, P., Ramesh, R., Hariharan, K., Kathiravan, C., & Gopalswamy, N. 2016, ApJ, 832, 59
Kishore, P., Ramesh, R., Kathiravan, C., & Rajalingam, M. 2015, SoPh, 290, 2409
Knock, S. A., & Cairns, I. H. 2005, JGRA, 110, A01101
Knock, S. A., Cairns, I. H., & Robinson, P. A. 2003, JGRA, 108, 1361
Komesaroff, M. 1958, AuJPh, 11, 201
Kouloumvakos, A., Rouillard, A., Warmuth, A., et al. 2021, ApJ, 913, 99
Kumari, A., Ramesh, R., Kathiravan, C., & Gopalswamy, N. 2017a, ApJ, 843, 10
Kumari, A., Ramesh, R., Kathiravan, C., Wang, T. J., & Gopalswamy, N. 2019, ApJ, 881, 24
Mancuso, S., Frassati, F., Bemporad, A., & Barghini, D. 2019, A&A, 624, L2
Mancuso, S., Raymond, J. C., Kohl, J., et al. 2003, A&A, 400, 347
Mann, G., Classen, T., & Aurass, H. 1995, A&A, 295, 775
McLean, D. J. 1967, PASA, 1, 47
Melrose, D. B., Dulk, G. A., & Gary, D. E. 1980, PASA, 4, 50
Melrose, D. B., & Sy, W. N. 1972, AuJPh, 25, 387
Monstein, C., Ramesh, R., & Kathiravan, C. 2007, BASI, 35, 473
Morosan, D. E., Räsänen, J. E., Kumari, A., et al. 2022, SoPh, 297, 47
Mugundhan, V., Hariharan, K., & Ramesh, R. 2017, SoPh, 292, 155
Mugundhan, V., Ramesh, R., Barve, I. V., et al. 2016, ApJ, 831, 154
Mugundhan, V., Ramesh, R., Kathiravan, C., et al. 2018a, ApJL, 855, L8
Mugundhan, V., Ramesh, R., Kathiravan, C., Gireesh, G. V. S., & Hegde, A. 2018b, SoPh, 293, 41
Nelson, G. J., & Melrose, D. B. 1985, in Solar Radiophysics: Studies of Emission from the Sun at Metre Wavelengths, ed. D. J. McLean & N. R. Labrum (Cambridge: Cambridge Univ. Press), 333
Nelson, G. J., & Robinson, R. D. 1975, PASA, 2, 370
Nelson, G. J., & Sheridan, K. V. 1974, in IAU Symp. 57, Coronal Disturbances, ed. G. A. Newkirk (Dordrecht: Reidel), 345
Newkirk, G., Jr. 1961, ApJ, 133, 983
Nindos, A., Alissandrakis, C. E., Hillaris, A., & Preka-Papadema, P. 2011, A&A, 531, A31
Pulupa, M., Bale, S. D., Badman, S. T., et al. 2020, ApJS, 246, 49
Ramesh, R. 2011, in Astron. Soc. India Conf. Ser. 2, 1st Asia-Pacific Sol. Phys. Meeting, ed. A. R. Choudhuri & D. Banerjee (Bangalore: BASI), 55
Ramesh, R., & Ebenezer, E. 2001, ApJL, 558, L141
Ramesh, R., Kathiravan, C., & Ebenezer, E. 2022b, ApJ, 932, 48
Ramesh, R., Kathiravan, C., Indrajit, V. B., & Rajalingam, M. 2012b, ApJ, 744, 165
Ramesh, R., Kathiravan, C., Sundara Rajan, M. S., Indrajit, V. B., & Rajalingam, M. 2014, in Astron. Soc. India Conf. Ser. 13, The Metrewavelength Sky, ed. J. N. Chengalur & Y. Gupta (Bangalore: BASI), 19
Ramesh, R., Kathiravan, C., Sundara Rajan, M. S., Indrajit, V. B., & Sastry, C. V. 2008, SoPh, 253, 319
Ramesh, R., Kathiravan, C., & Surya Natarajan, S. 2022a, ApJ, 926, 38
Ramesh, R., Kumari, A., Kathiravan, C., et al. 2020b, GeoRL, 47, e90426
Ramesh, R., Nataraj, H. S., Kathiravan, C., & Sastry, C. V. 2006a, ApJ, 648, 707
Ramesh, R., & Sastry, C. V. 2000, A&A, 358, 749
Ramesh, R., & Sastry, C. V. 2005, in ASP Conf. Ser. 346, Large-scale Structures and their Role in Solar Activity, ed. K. Sankarasubramanian, M. Penn, & A. Pevtsov (San Francisco, CA: ASP), 153
Ramesh, R., Subramanian, K. R., & Sastry, C. V. 1999a, A&AS, 139, 179
Ramesh, R., Subramanian, K. R., & Sastry, C. V. 1999b, SoPh, 185, 77
Ramesh, R., Subramanian, K. R., Sundara Rajan, M. S., & Sastry, C. V. 1998, SoPh, 181, 439
Ramesh, R., Sundara Rajan, M. S., & Sastry, C. V. 2006b, ExA, 21, 31
Roberts, J. A. 1959, AuJPh, 12, 327
Saito, K., Poland, A. I., & Munro, R. H. 1977, SoPh, 55, 121
Sasikumar Raja, K., Kathiravan, C., Ramesh, R., Rajalingam, M., & Indrajit, V. B. 2013a, ApJS, 207, 2
Sastry, C. 1994, SoPh, 150, 285
Singh, J., Raghavendra Prasad, B., Venkatakrishnan, P., et al. 2011, CSci, 100, 167
Smerd, S. F., Sheridan, K. V., & Stewart, R. T. 1974, in IAU Symp. 57, Coronal Disturbances, ed. G. A. Newkirk (Dordrecht: Reidel), 389
Smerd, S. F., Sheridan, K. V., & Stewart, R. T. 1975, ApL, 16, 23
Stewart, R. T. 1966, AuJPh, 19, 209
Su, W., Li, T. M., Cheng, X., et al. 2022, ApJ, 929, 175
Suzuki, S., Stewart, R. T., & Magun, A. 1980, in IAU Symp. 86, Radiophysics of the Sun, ed. M. R. Kundu & T. E. Gergely (Dordrecht: Reidel), 245
Thejappa, G., & Kundu, M. R. 1991, SoPh, 132, 173
Thejappa, G., & MacDowall, R. J. 2008, ApJ, 676, 1338
Thejappa, G., Zlobec, P., & MacDowall, R. J. 2003, ApJ, 592, 1234
Vrsnak, B., Aurass, H., Magdalenic, J., & Gopalswamy, N. 2001, A&A, 377, 321
Vrsnak, B., Magdalenic, J., Aurass, H., & Mann, G. 2002, A&A, 396, 673
Vrsnak, B., Magdalenic, J., & Zlobec, P. 2004, A&A, 413, 753
Willes, A. J., & Melrose, D. B. 1997, SoPh, 171, 393
Zhang, P., Zucca, P., Kozarev, K., et al. 2022, ApJ, 932, 17
Zimovets, I., Vilmer, N., Chian, A.-C.-L., Sharykin, I., & Struminsky, A. 2012, A&A, 547, A6
Zimovets, I. V., & Sadykov, V. M. 2015, AdSpR, 56, 2811
Zlotnik, E. Y. 1981, A&A, 101, 250
Zucca, P., Pick, M., Demoulin, P., et al. 2014, ApJ, 795, 68